Supplementary Information

Pulsed laser deposition of highly oriented Sb_2Te_3 and GeTe-Sb_2Te_3 thin films on amorphous SiO_x layers at low temperatures

Sonja Cremer,[a,*] Nils Braun,[a] Lennart Voß,[c] Jens Bauer,[a] Vladimir Roddatis,[b] Lorenz Kienle,[c,d] and Andriy Lotnyk [a,*]

[a]Leibniz Institute of Surface Engineering (IOM), Permoserstr. 15, 04318 Leipzig, Germany

[b]GFZ Helmholtz Centre for Geosciences, Telegrafenberg, 14473 Potsdam, Germany

[c]Department of Material Science, Kiel University, Kaiserstr. 2, 24143 Kiel, Germany

[d]Kiel Nano, Surface and Interface Science (KiNSIS), Kiel University, Christian-Albrechts-Platz 4, 24118 Kiel, Germany

*Corresponding authors: sonja.cremer@iom-leipzig.de, andriy.lotnyk@iom-leipzig.de

In situ heating and cooling procedures

Heating and cooling curves were determined in a separate measurement performed using an Optrics PI OPTPI1606T900 IR camera and Optrics PIX Connect V3.22.3118.0 software. For this purpose, the same native SiO_x/Si substrate ($\rho < 0.01\ \Omega$ cm) as used for the Sb_2Te_3 samples was subjected to the same heating and cooling procedure as during the preparation of the thin films. The chamber pressure measured around 5 x 10^{-7} mbar. Prior, calibration measurements with the Si substrate were performed. Figure S1 displays the heating and cooling curves of sample 6 – 9. The remaining samples were also subjected to one of these four heating procedures (Table S1). The deposition of the samples

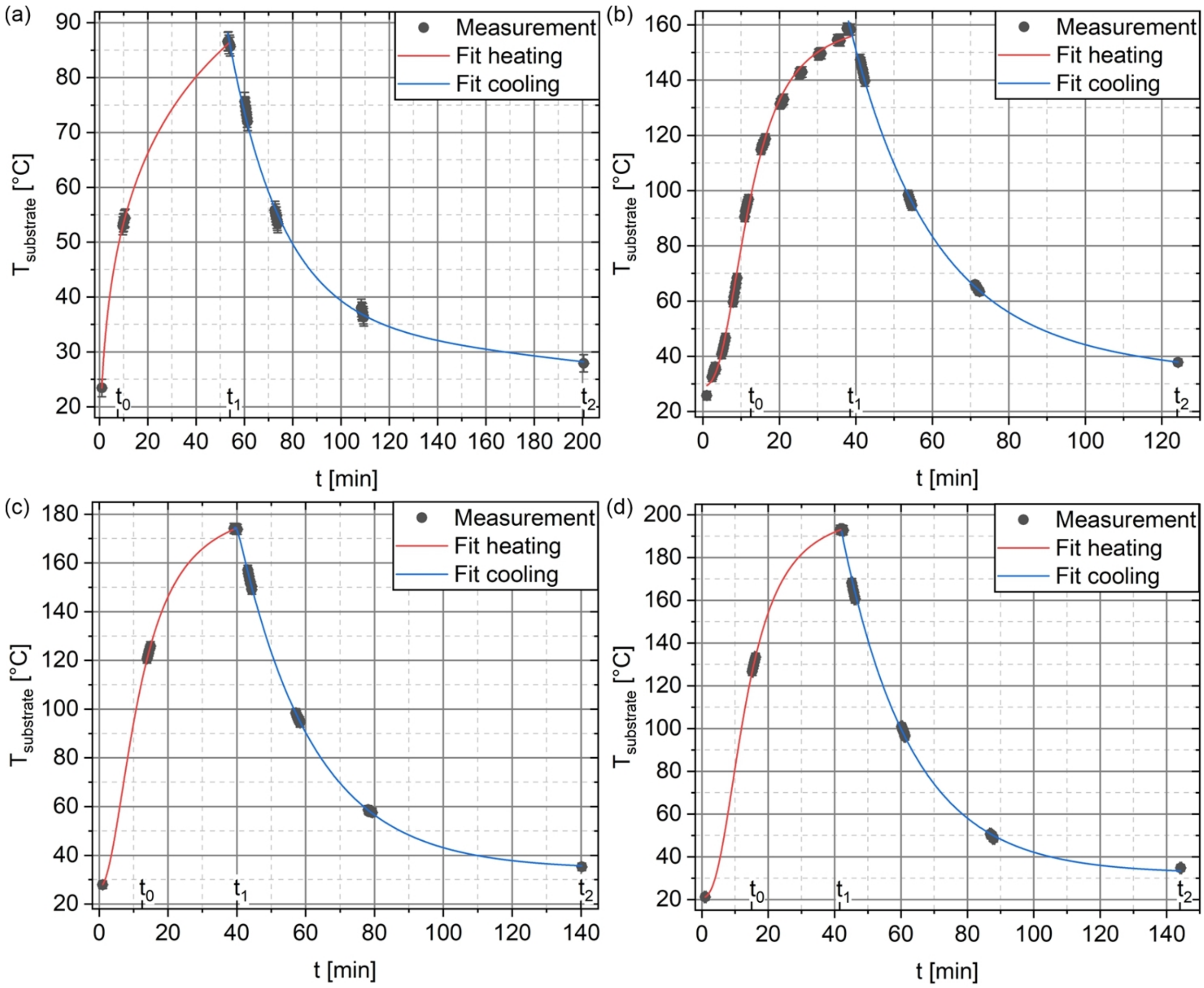

Figure S1: Heating ($0 \leq t \leq t_1$) and cooling curves ($t_1 \leq t \leq t_2$) for (a) sample 6, (b) sample 7, (c) sample 8, (d) sample 9. Deposition of seed layer started at $t = t_0$. Annealing of the thin film as last step was completed at $t = t_{end} = t_1$.

always started at t = t_0. As different deposition and annealing steps were used, the samples were fully prepared at different t_{end} resulting in different temperatures during the preparation as indicated in Table 1.

Table S1: Heating procedures used for sample preparation.

Sample	1	2	3	4	5	6	7	8	9	10	11	12
Figure	S1(b)	S1(b)	S1(b)	S1(c)	S1(d)	S1(a)	S1(b)	S1(c)	S1(d)	S1(a)	S1(b)	S1(b)
t_{end} [min]	22.5	23	39.5	29.5	31.5	54	39	39.5	41.5	53.5	38.5	28.5

Supplementary figures

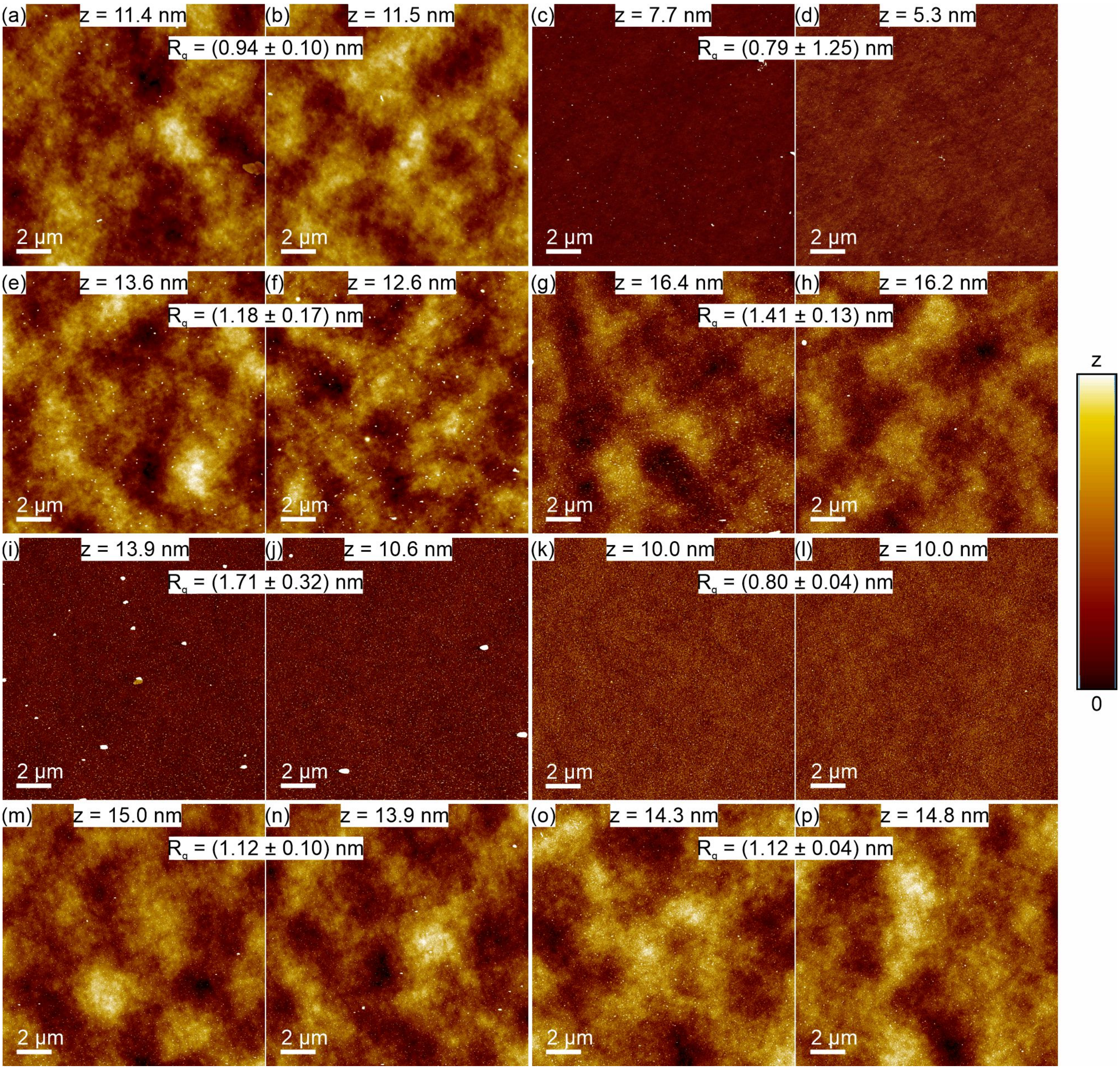

Figure S2: AFM images of (a), (b) sample 1, (c), (d) sample 2, (e), (f) sample 6, (g), (h) sample 7, (i), (j) sample 8 and (k), (l) sample 9, (m), (n) sample 11 and (o), (p) sample 12.

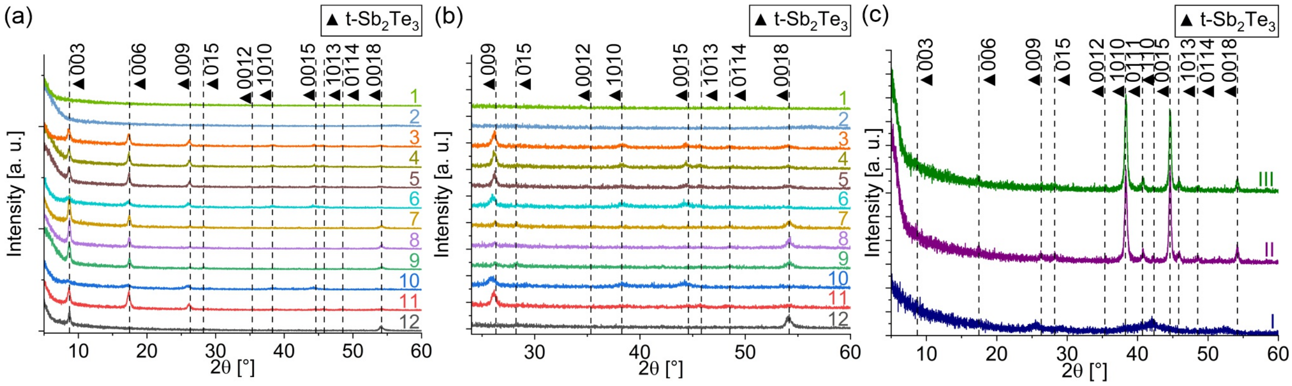

Figure S3: (a) GID scans of the samples 1 – 12, (b) zoom graph of the diffractograms of (a) in the higher 2θ range, (c) GID-scans of the ex situ heated sample in state I – III.

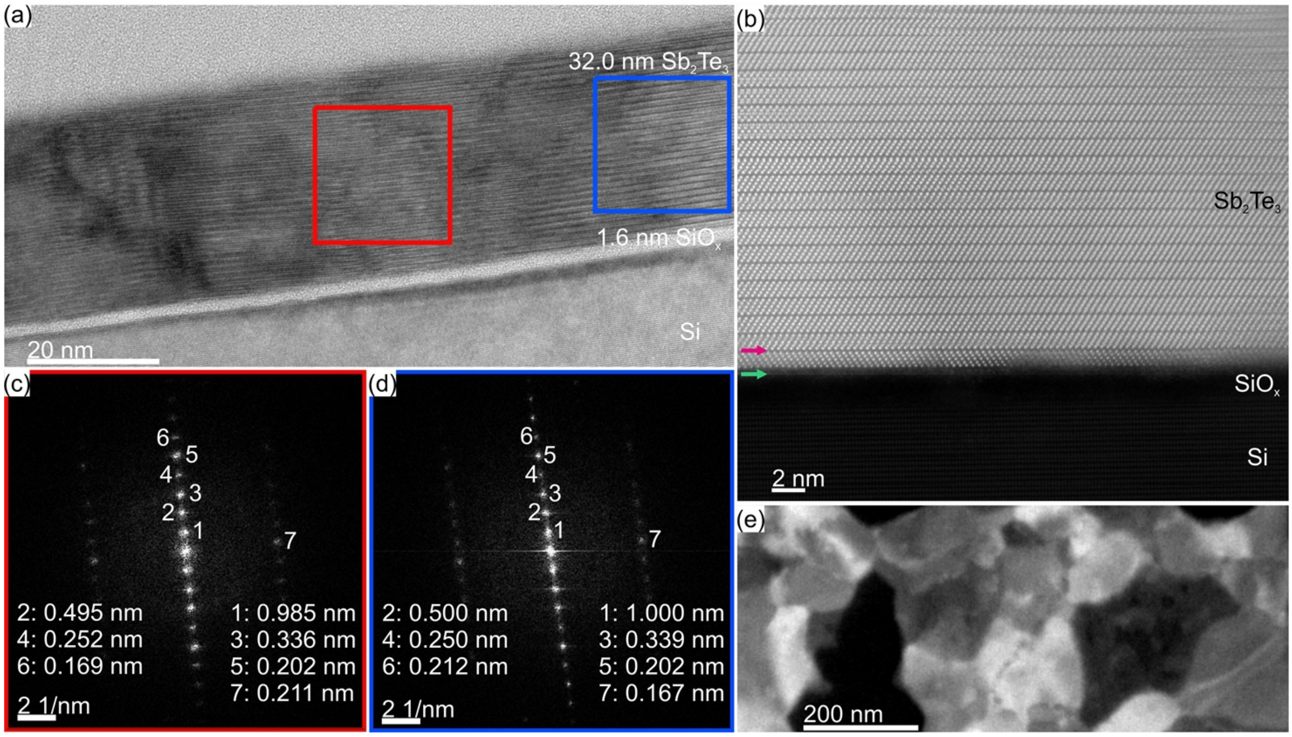

Figure S4: TEM/STEM analysis of sample 12. (a) TEM micrograph. The error for layer thickness determination was estimated to 0.6 nm. (b) HAADF-STEM image of the substrate-layer interface with pink arrow marking a twin boundry and green arrow indicating sporatically formed passivation layer. (c, d) FFTs of the regions marked with the red and blue rectangle in (a), respectively. (e) Plane-view HAADF-STEM image. Black areas in (e) are artefacts introduced by specimen preparation.

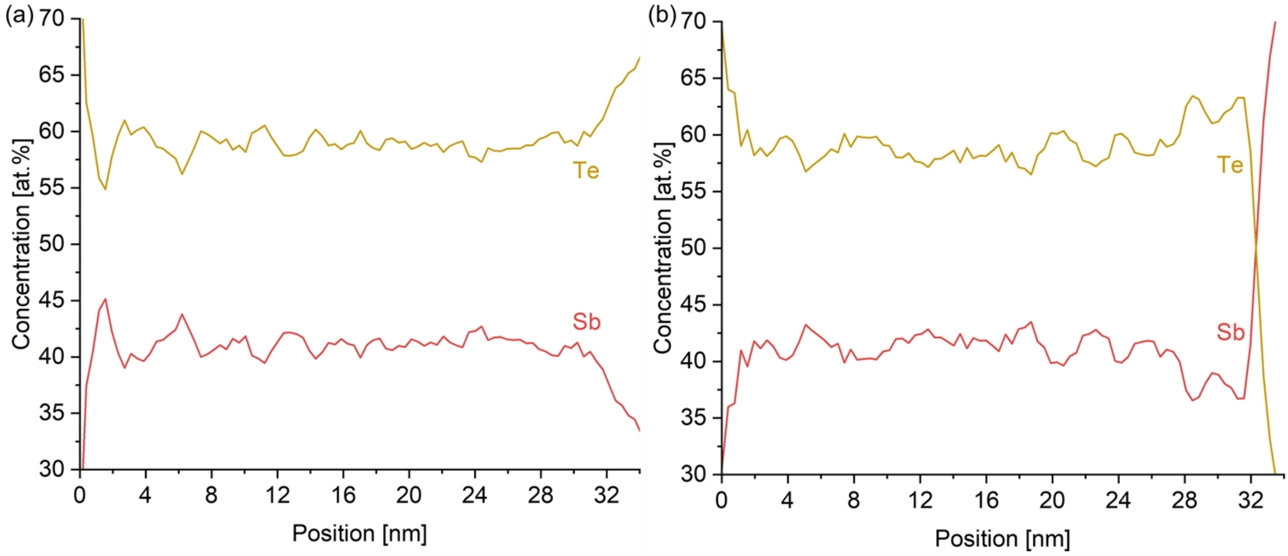

Figure S5: EDX line scan of (a) sample 11 and (b) sample 12. The substrate-layer interface is located at 0 nm position, respectively.

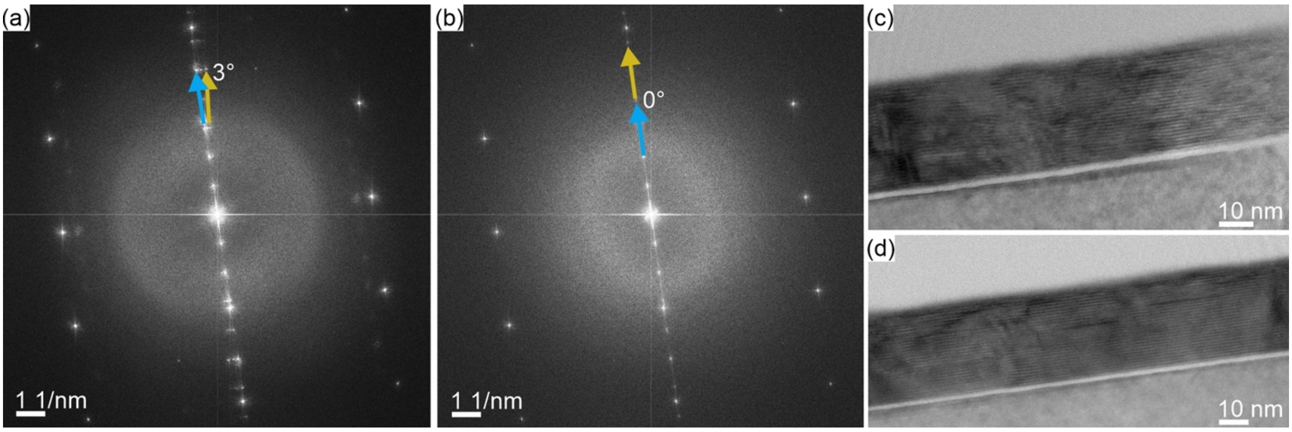

Figure S6: (a) FFT of TEM image in (c), (b) FFT of TEM image in (d) used for investigation of the grain tilt of sample 12. The blue arrow marks [111] Si and the yellow arrow indicates [001] Sb_2Te_3.

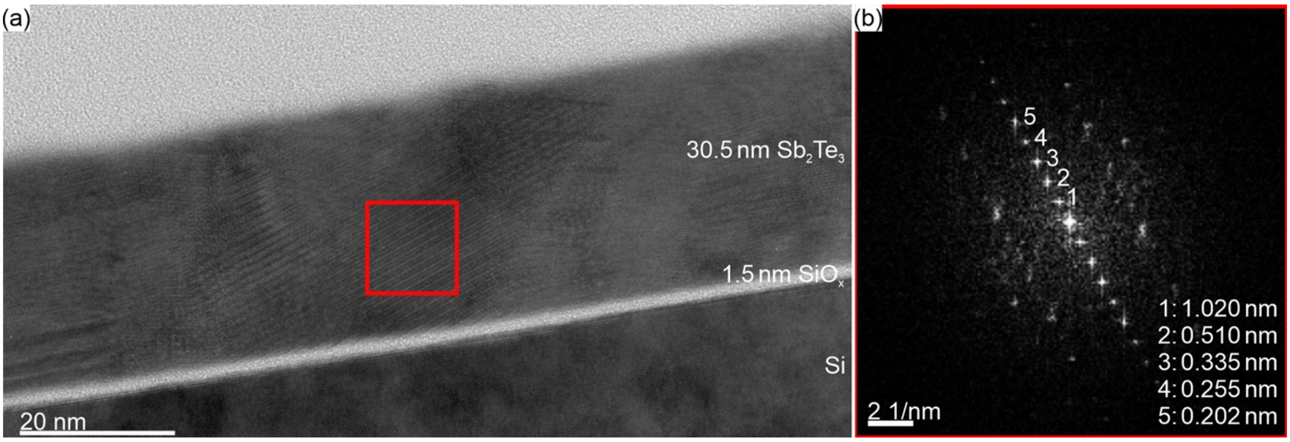

Figure S7: (a) TEM micrograph of sample 6 and (b) FFT of the region marked with the red rectangle in (a). The error for layer thickness determination was estimated to 0.6 nm.

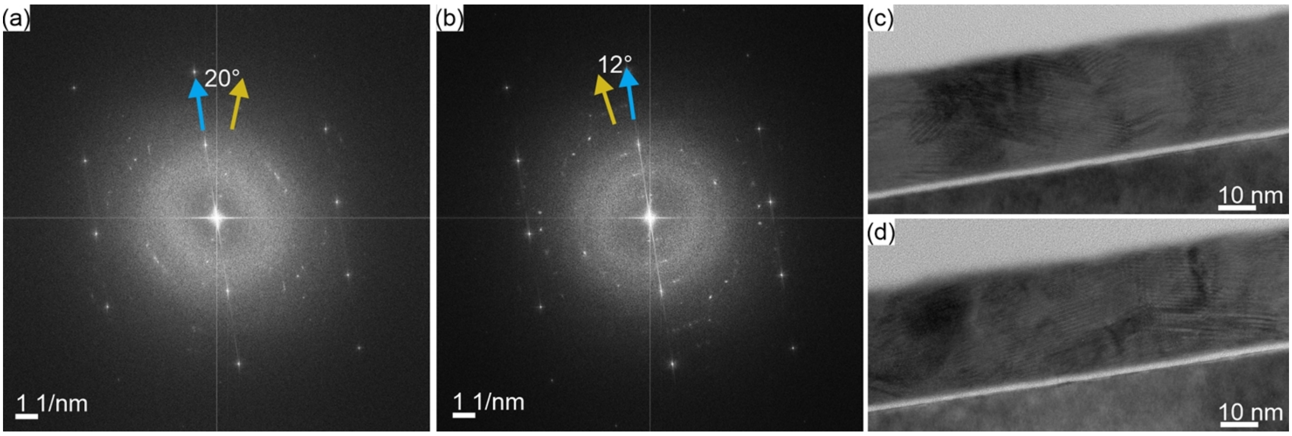

Figure S8: (a) FFT of TEM image in (c), (b) FFT of TEM image in (d) used for investigation of the grain tilt of sample 6. The blue arrow marks [111] Si and the yellow arrow indicates [001] Sb_2Te_3.

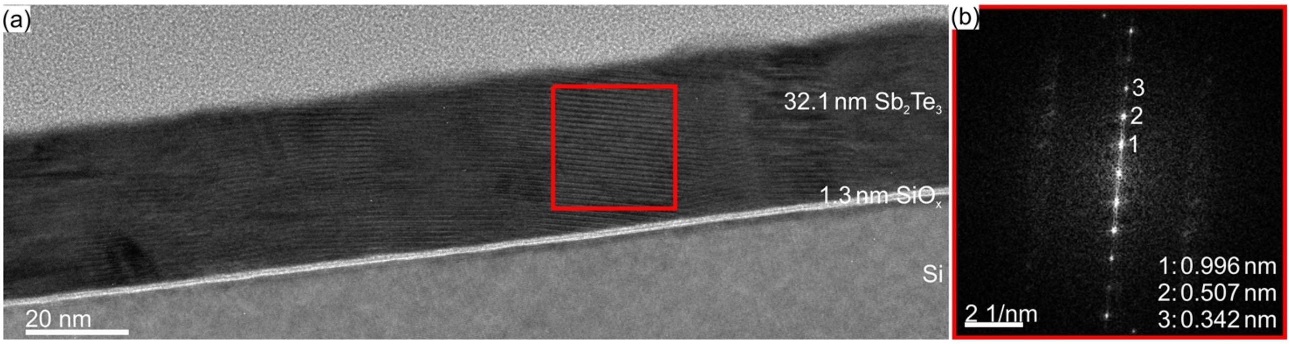

Figure S9: (a) TEM micrograph of sample 3 and (b) FFT of the region marked with the red rectangle in (a). The error for layer thickness determination was estimated to 0.6 nm.

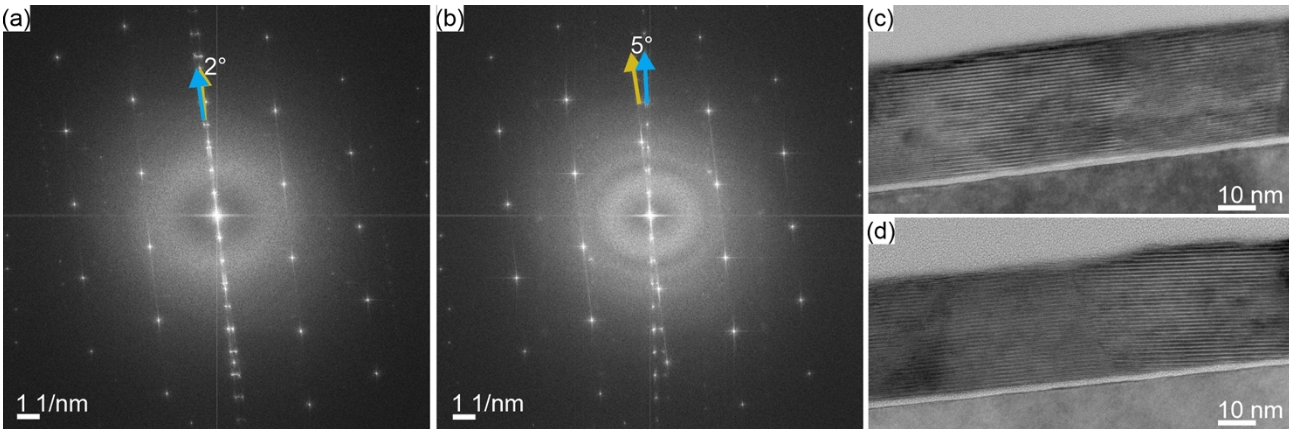

Figure S10: (a) FFT of TEM image in (c), (b) FFT of TEM image in (d) used for investigation of the grain tilt of sample 7. The blue arrow marks [111] Si and the yellow arrow indicates [001] Sb_2Te_3.

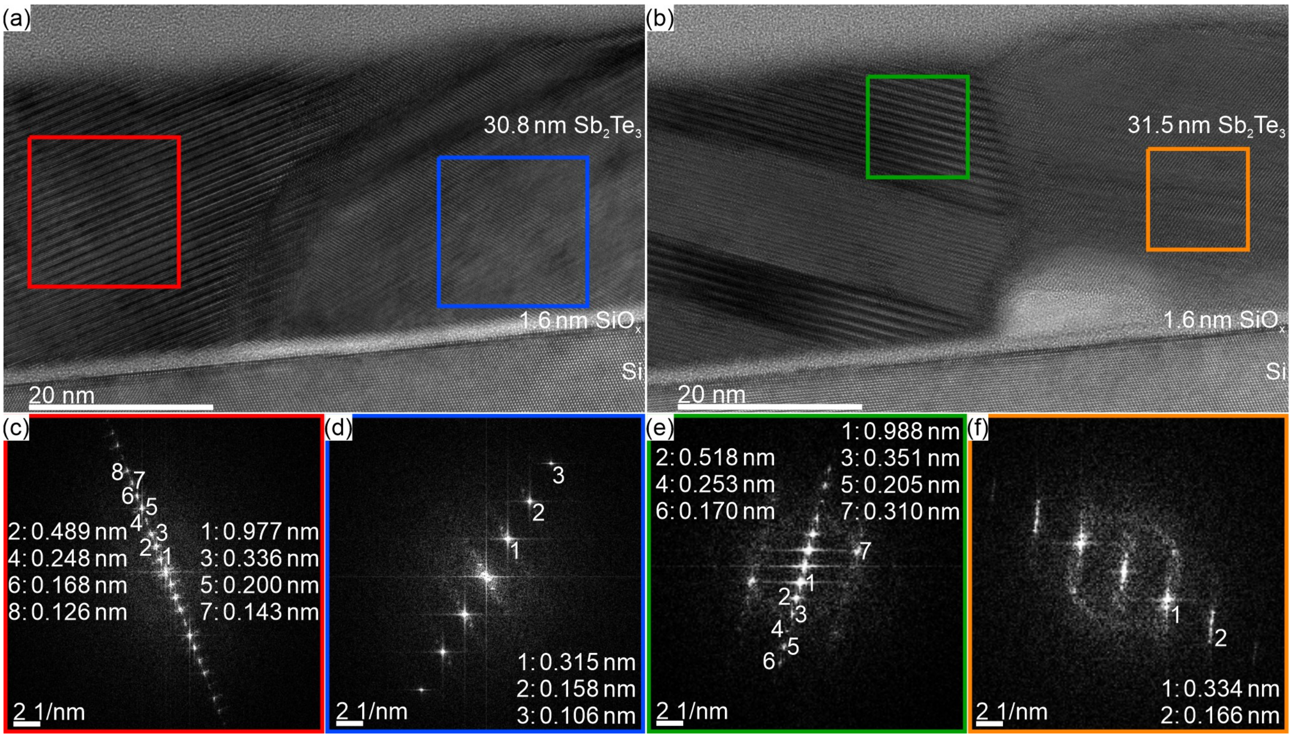

Figure S11: (a), (b) TEM micrographs of *ex-situ* heated Sb_2Te_3 layer in state III. (c)-(f) FFTs of the regions marked by the color-coded rectangles in (a) and (b), respectively. The error for layer thickness determination was estimated to 0.6 nm. It should be noted that the presence of voids at the Sb_2Te_3-SiO_x interface points out to volume diffusion. In addition, the voids are observed at the junction of two grains. It is probable that out diffusion of Sb and Te occurs throughout the grain boundaries.

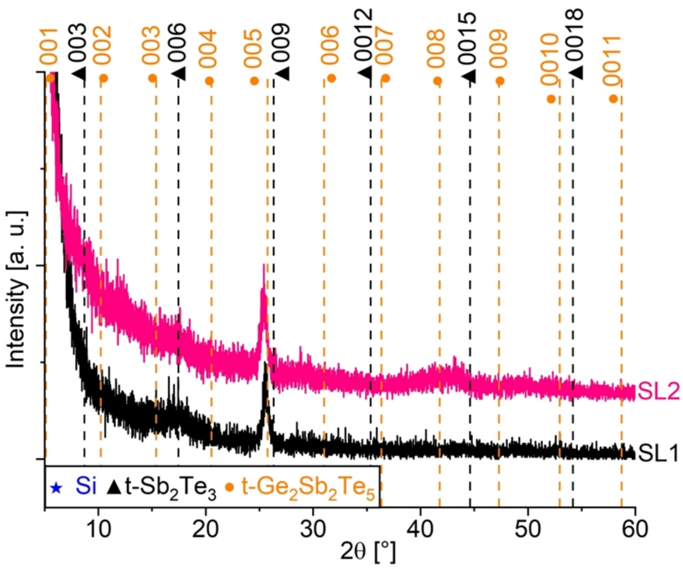

Figure S12: GID scans of SL1 and SL2 samples.

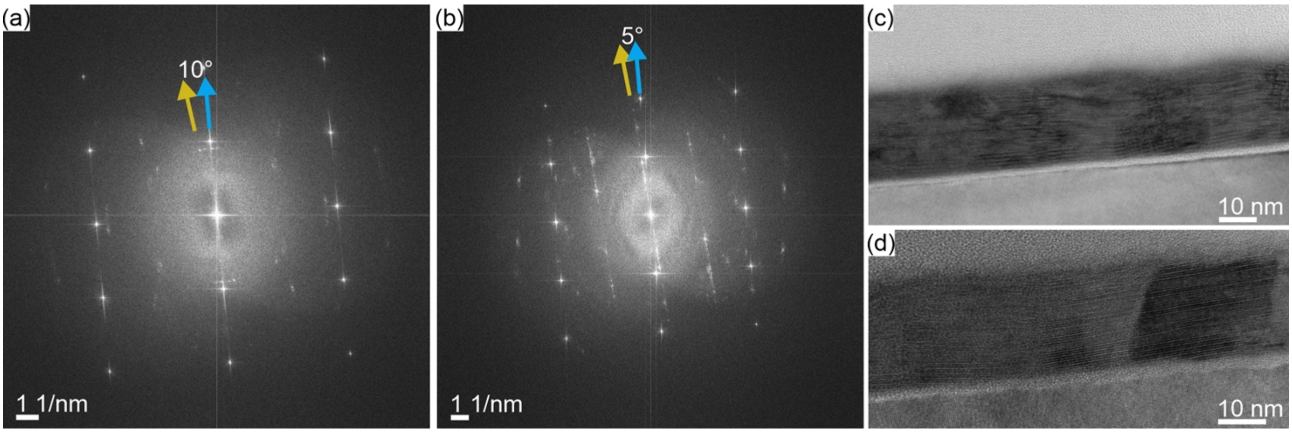

Figure S13: (a) FFT of TEM image in (c), (b) FFT of TEM image in (d) used for investigation of the grain tilt of SL1. The blue arrow marks [111] Si and the yellow arrow indicates [001] Sb_2Te_3.

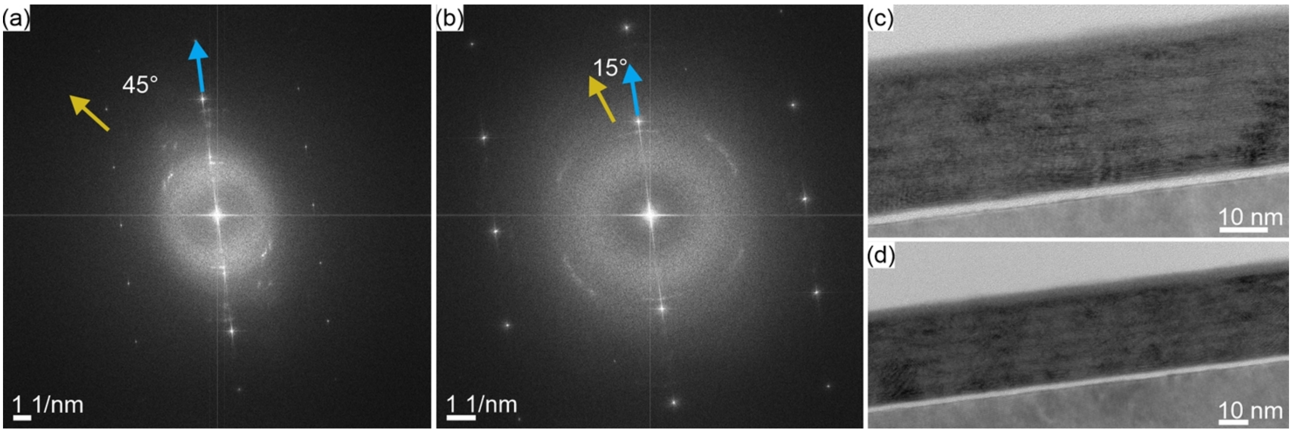

Figure S14: (a) FFT of TEM image in (c), (b) FFT of TEM image in (d) used for investigation of the grain tilt of SL2. The blue arrow marks [111] Si and the yellow arrow indicates [001] Sb_2Te_3.

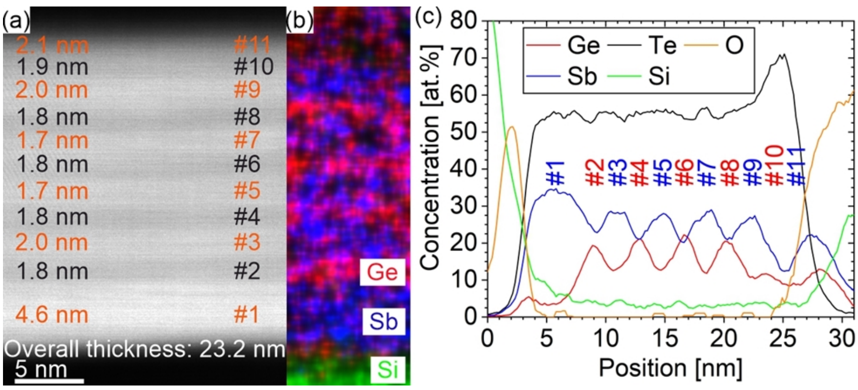

Figure S15: (a) Overview RDF processed HAADF-STEM image of SL1. The error for layer thickness determination was estimated to 0.3 nm. (b) EDX map and (c) EDX line scan of SL1.

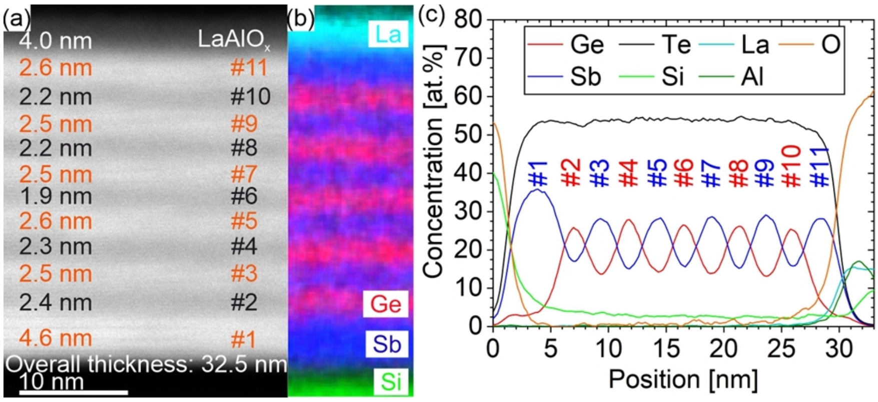

Figure S16: (a) Overview RDF processed HAADF-STEM image of SL2. The error for layer thickness determination was estimated to 0.3 nm. (b) EDX map and (c) EDX line scan of SL2.